

Spin-Boson Hamiltonian and Optical Absorption of Molecular Dimers

Christiane Koch* and Bernd Esser†

*Institut für Physik, Humboldt-Universität zu Berlin, Invalidenstr. 110,
D-10115 Berlin, Germany*

(November 11, 2018)

An analysis of the eigenstates of a symmetry-broken spin-boson Hamiltonian is performed by computing Bloch and Husimi projections. The eigenstate analysis is combined with the calculation of absorption bands of asymmetric dimer configurations constituted by monomers with nonidentical excitation energies and optical transition matrix elements. Absorption bands with regular and irregular fine structures are obtained and related to the transition from the coexistence to a mixing of adiabatic branches in the spectrum. It is shown that correlations between spin states allow for an interpolation between absorption bands for different optical asymmetries.

I. INTRODUCTION

The spectral properties of the spin-boson Hamiltonian have frequently been addressed in the past and in the last years investigations on the spectral features of classical nonintegrability in the quantum case were performed (see e.g. [1–4] and references therein). The interest in the spectral and dynamical properties of the spin-boson Hamiltonian is due to its numerous applications which include a large variety of phenomena in molecular and solid state physics with one realization being the optical and transfer properties of excitonic-vibronic coupled dimers. Thus the spectral and related optical properties of the corresponding dimer Hamiltonian have intensively been investigated over the years, as examples we point to the work exposed in [5,6]. Most of these investigations were based on a Hamiltonian corresponding to a symmetric dimer configuration. However, from the point of view of a general asymmetric situation the symmetric case is singular, e.g. the quantum states possess parity properties in the symmetric case, which are not present in general. It should be noted that dimers often constitute subunits of more complicated molecular aggregates with an asymmetric structure, which breaks the symmetry of the dimer configuration (see e.g. [7]). Therefore the aim of this paper is to go beyond the symmetric case and to connect the properties of the eigenstates of a generalized and symmetry-broken spin-boson Hamiltonian with the line spectrum of absorption bands of asymmetric excitonic-vibronic coupled molecular dimers.

We combine a phase space analysis of the eigenstates, which is based on the method of Husimi projections [8], with the calculation of the matrix elements of optical transitions. Husimi projections have repeatedly been used in order to establish the features of nonintegrability of classical systems in the corresponding quantum case [1,9,10]. Analyzing the Husimi projections of the eigenstates of the spin-boson Hamiltonian in relation to optical transitions we indicate a bridge between the eigenstate analysis of nonintegrable systems and observables in an optical experiment. In particular, we show how the intensity variations in the Husimi projections are related to the spectral randomness in the fine structure of absorption bands. Such spectral randomness in the eigenstates of the spin-boson Hamiltonian is also known as incipience of quantum chaos [11–13]. In this case random features of the spectrum are just appearing while the system is still far from displaying universal spectral fluctuations described by random matrix theory and known for excited states of spectra of polyatomic molecules [14].

A central point in our eigenstate analysis will be to find out to what extent the adiabatic reference systems of the spin-boson Hamiltonian are present in its exact eigenstates and how the appearance of spectral randomness can be interpreted as a mixing of such reference systems. Following [13] we show that Bloch projections are a useful quantitative characteristic to describe this mixing. Computing the Bloch projections of the eigenstates, it is possible to distinguish the spectral region where the adiabatic branches of the spectrum are still intact from the region with a substantial mixing of adiabatic reference systems. Furthermore, by performing projections of the numerically obtained eigenstates onto the ground state we obtain the details of the fine structure of the absorption bands in the spectral

*Present address: Fritz-Haber-Institut der Max-Planck-Gesellschaft, Abt. Chemische Physik, Faradayweg 4-6, 14195 Berlin, Germany

†Corresponding author. Fax 49 30 2093 7638; e-mail: bernd.esser@physik.hu-berlin.de

regions as indicated by the Franck-Condon principle. We note that the asymmetric case has some special features, which are not present in the symmetric situation: In the asymmetric case the final states of an optical transition can be located in the higher energetic regions of the corresponding adiabatic potentials. Then, as will be shown below for two representative cases, the fine structure of the spectrum and of the absorption bands can greatly vary from regular to irregular arrangements of absorption lines.

The paper is organized as follows: In Sec.II the model and the basic equations are presented. In Sec.III the eigenstate analysis for two representative cases of the asymmetric spin-boson Hamiltonian is performed and in Sec.IV this analysis is connected with the properties of the absorption bands in the corresponding spectral regions. Finally, in Sec.V our conclusions are summarized.

II. MODEL

We consider a dimer system described by the Hamiltonian

$$\hat{H} = \sum_n (\epsilon_n + \gamma_n q_n) |n\rangle \langle n| + \sum_{\substack{n,m \\ n \neq m}} V_{nm} |n\rangle \langle m| + \sum_n \frac{1}{2} (p_n^2 + \omega_n^2 q_n^2), \quad (1)$$

where $|n\rangle$ ($|m\rangle$) are the excited states of the molecular monomers constituting the dimer ($n, m = 1, 2$) with the excitonic energies ϵ_n , the coupling constants to intramolecular vibrations γ_n and the transfer matrix element V_{nm} . The variables q_n , p_n and ω_n represent coordinate, momentum and frequency of the vibrations, respectively. The coupling of the excited dimer states to an incident light wave with electrical field vector $\vec{E}_n(t)$ is given by

$$\hat{H}_{int} = \sum_n \vec{\mu}_n \vec{E}_n(t) |n\rangle \langle 0|, \quad (2)$$

where $\vec{\mu}_n$ and $\vec{E}_n(t)$ are the optical transition matrix element and electric field at the n th monomer, respectively, and $|0\rangle$ is the excitonic vacuum. We consider an asymmetric configuration of the dimer system by assuming different monomer energies ϵ_n and optical transition matrix elements $\vec{\mu}_n$. In order to keep the number of asymmetry parameters minimal we assume symmetric transfer rates, $V_{nm} = V_{mn} = -V$, $V > 0$, and equal coupling constants and frequencies, i.e. $\gamma_1 = \gamma_2 = \gamma$ and $\omega_1 = \omega_2 = \omega$. Then the coupling can be reduced to a single vibrational mode by introducing the relative displacement of the vibrations.

The Hamiltonian (1) can be represented as an operator in the space of two-dimensional vectors $C = \begin{pmatrix} c_1 \\ c_2 \end{pmatrix}$ using the standard Pauli spin matrices $\hat{\sigma}_i$ ($i = x, y, z$). Passing to dimensionless variables by measuring the energy in units of $2V$, $H = H/2V$, one obtains from (1) the spin-boson Hamiltonian

$$\hat{H} = \epsilon_+ \mathbb{1} - \frac{1}{2} \hat{\sigma}_x + \frac{1}{2} (\hat{P}^2 + r^2 \hat{Q}^2) \mathbb{1} + (\sqrt{\frac{p}{2}} r \hat{Q} + \epsilon_-) \hat{\sigma}_z. \quad (3)$$

In (3), the dimensionless relative displacement and corresponding momentum, to which the exciton is coupled, are given by $\hat{Q} = \sqrt{2V}(\hat{q}_1 - \hat{q}_2)$ and $\hat{P} = (\hat{p}_1 - \hat{p}_2)/\sqrt{2V}$. The dimensionless parameters of the spin-boson Hamiltonian (3) are related to the dimer system (1) by

$$p = \frac{\gamma^2}{2V\omega^2}, \quad (4)$$

$$r = \frac{\omega}{2V}, \quad (5)$$

$$\epsilon_{\pm} = \frac{\epsilon_1 \pm \epsilon_2}{4V}. \quad (6)$$

The parameter p expresses the coupling strength, and r is the adiabatic parameter measuring the relative strength of quantum effects of the subsystems. The sum ϵ_+ represents the center of the excitation energy, whereas the difference ϵ_- is the asymmetry parameter. For $\epsilon_- = 0$, one obtains the symmetric spin-boson Hamiltonian with conservation of total parity (given by the operation $\hat{Q} \rightarrow -\hat{Q}$, $\hat{\sigma}_z \rightarrow -\hat{\sigma}_z$). For $\epsilon_- \neq 0$, this symmetry is broken.

The adiabatic reference systems associated with (3) are introduced by considering the eigenvalue problem of the adiabatic part \hat{h}_{ad} ,

$$\hat{h}_{\text{ad}} = -\frac{1}{2}\hat{\sigma}_x + \left(\sqrt{\frac{p}{2}}rQ + \epsilon_{-}\right)\hat{\sigma}_z + \frac{r^2}{2}Q^2\mathbb{1}. \quad (7)$$

The Q -dependent eigenvalues and eigenstates of \hat{h}_{ad} are easily obtained. In particular, one finds the two adiabatic potentials $U_{\text{ad}}^{\pm}(Q)$ for the upper (+) and lower (-) states

$$U_{\text{ad}}^{\pm}(Q) = \frac{r^2}{2}Q^2 \pm \sqrt{\frac{1}{4} + \left(\epsilon_{-} + \sqrt{\frac{p}{2}}rQ\right)^2}, \quad (8)$$

from which the Hamiltonians of the adiabatic reference systems are obtained

$$H^{\pm}(Q) = \frac{1}{2}P^2 + U_{\text{ad}}^{\pm}(Q). \quad (9)$$

A key point in our analysis of the eigenstates and absorption bands will be the extent to which the exact eigenstates of the Hamiltonian (3) can be viewed as a mixing of adiabatic reference systems connected with the adiabatic Hamiltonians (9). As is shown below, the extent of this mixing can be controlled by analyzing Husimi projections and by computing Bloch projections from the numerically obtained eigenstates. Husimi projections constitute phase space representations of the eigenstates which can be compared with the phase space orbits of the adiabatic reference systems (9). Bloch projections constitute another independent indicator of the mixing of the adiabatic branches in the spectrum. For the adiabatic branches these projections are calculated from the eigenstates of the Hamiltonian (7)

$$|\varphi_{\text{ad}}^{+}(Q)\rangle = \frac{1}{\sqrt{2}} \left(\sqrt{1+A(Q)}|\uparrow\rangle - \sqrt{1-A(Q)}|\downarrow\rangle \right) \quad (10a)$$

$$|\varphi_{\text{ad}}^{-}(Q)\rangle = \frac{1}{\sqrt{2}} \left(\sqrt{1-A(Q)}|\uparrow\rangle + \sqrt{1+A(Q)}|\downarrow\rangle \right) \quad (10b)$$

where

$$A(Q) = \frac{2\epsilon_{-} + \sqrt{2pr}Q}{\sqrt{1 + (2\epsilon_{-} + \sqrt{2pr}Q)^2}}. \quad (11)$$

Computing the expectation values $x = \langle\hat{\sigma}_x\rangle$ of the Pauli matrix $\hat{\sigma}_x$ for the adiabatic eigenstates (10), one obtains the Bloch projections of the adiabatic branches

$$\langle\varphi_{\text{ad}}^{\pm}(Q)|\hat{\sigma}_x|\varphi_{\text{ad}}^{\pm}(Q)\rangle = \mp \frac{1}{\sqrt{1 + (2\epsilon_{-} + \sqrt{2pr}Q)^2}}, \quad (12)$$

According to eq.(12) there is a distinction in the sign of the Bloch projections for the adiabatic eigenstates. Computing the Bloch projections from the numerically obtained eigenstates this distinction in the sign will be used as an indicator for the case in which the spectrum resolves into adiabatic branches.

III. EIGENSTATE ANALYSIS

Our analysis is based on a diagonalization of the spin-boson Hamiltonian using a basis of product states of spin states with harmonic oscillator eigenstates. In this basis the eigenstates are obtained in the form

$$|\lambda\rangle = \sum_m \left(c_{\uparrow m}^{(\lambda)}|\uparrow\rangle + c_{\downarrow m}^{(\lambda)}|\downarrow\rangle \right) |m\rangle = \sum_m \left| s_m^{(\lambda)} \right\rangle |m\rangle, \quad (13)$$

where $|\uparrow\rangle = \begin{pmatrix} 1 \\ 0 \end{pmatrix}$, $|\downarrow\rangle = \begin{pmatrix} 0 \\ 1 \end{pmatrix}$ denote the spin up (down) states, $|m\rangle$ the harmonic oscillator eigenstates and $c_{zm}^{(\lambda)}$ ($z = \uparrow, \downarrow$) the expansion coefficients of the λ eigenstate. For a fixed m we will also use the spin representation $\left| s_m^{(\lambda)} \right\rangle$ for the up and down coefficients $c_{zm}^{(\lambda)}$ ($z = \uparrow, \downarrow$) for a given oscillator state as indicated in the second part of (13). The matrix dimension in the numerical diagonalization was $N = 4000$, for the eigenstate analysis the first 1100 eigenstates were used.

For the phase space representation of the eigenstates Husimi projections are used. Husimi projections $h_\lambda(\alpha(Q, P); s)$ are defined by projecting an eigenstate $|\lambda\rangle$ onto a set of coherent oscillator states $|\alpha(Q, P)\rangle$, which scan the oscillator phase plane of the vibrational subsystem, while the spin projection $|s\rangle = c_\uparrow|\uparrow\rangle + c_\downarrow|\downarrow\rangle$ is kept fixed,

$$h_\lambda(\alpha(Q, P); s) = |\langle \lambda | \alpha(Q, P), s \rangle|^2, \quad (14)$$

and $|\alpha(Q, P), s\rangle = |\alpha(Q, P)\rangle|s\rangle$. Using the explicit form of $|\lambda\rangle$ in (13) one finds

$$h_\lambda(\alpha(Q, P); s) = \left| \sum_m (c_{\uparrow m}^{*(\lambda)} c_\uparrow + c_{\downarrow m}^{*(\lambda)} c_\downarrow) \langle m | \alpha(Q, P) \rangle \right|^2, \quad (15)$$

where $\langle m | \alpha(Q, P) \rangle = \frac{\alpha^m}{\sqrt{m!}} e^{-\frac{|\alpha|^2}{2}}$ and $\alpha(Q, P) = \sqrt{\frac{r}{2}} \langle \hat{Q} \rangle + \frac{i}{\sqrt{2r}} \langle \hat{P} \rangle$.

For the Bloch projection of an eigenstate,

$$x_\lambda = \langle \lambda | \hat{\sigma}_x | \lambda \rangle, \quad (16)$$

one finds from the expansion (13)

$$x_\lambda = \sum_m \left(c_{\uparrow m}^{*(\lambda)} c_{\downarrow m}^{(\lambda)} + c_{\downarrow m}^{*(\lambda)} c_{\uparrow m}^{(\lambda)} \right). \quad (17)$$

Before turning to the eigenstate analysis for definite parameter sets we note that the appearance of spectral irregularities can be expected in the high energetic region of the overlap of both adiabatic potentials only, where a sufficient number of states of both potentials mix. It is obvious that such a region can be probed by the final states of an optical transition in the asymmetric case only: In the symmetric case, as is evident from the adiabatic potentials (8), the optical transitions would necessarily terminate in the ground state region of the upper potential, where only a few states of the upper potential can mix with the lower potential. Therefore when investigating the structure of the spectrum and eigenstates of the spin-boson Hamiltonian we paid special attention to a systematic change of the asymmetry parameter ϵ_- combined with the coupling parameter p in order to produce appropriate configurations of the adiabatic potentials. Such configurations were found for relatively high coupling p and asymmetry values ϵ_- . Below we present the eigenstate analysis for two typical asymmetric configurations in the adiabatic parameter region ($r < 1$) with the parameter sets

A: $p = 4$, $r = 0.1$ and $\epsilon_- = 5$ and

B: $p = 20$, $r = 0.1$ and $\epsilon_- = 10$.

The parameter set B corresponds to a stronger coupling value p and a larger asymmetry parameter ϵ_- , as compared to set A. To indicate the location of the absorption bands, which will be analyzed in section IV, the adiabatic potentials of set B and the ground state of the system are shown in Fig. 1.

In Fig. 2 we start with the eigenstate analysis for the parameter set A by displaying the Bloch projections $x(E_\lambda)$ computed from the eigenstates according to eq.(17). In the low energy region one finds one adiabatic branch in the $x(E_\lambda)$ dependence associated with the lower adiabatic potential (for which $x_\lambda > 0$ in accordance with the sign in (12)). The overlap of the two potentials is marked by the appearance of a second adiabatic branch in the $x(E_\lambda)$ dependence. The mixing of the eigenstates of the two adiabatic potentials is seen by the disappearance of both adiabatic branches and indicated by a broad band of Bloch projections in the high energy region. The presence of three characteristic regions in the Bloch projections with one adiabatic branch, two adiabatic branches and the mixing region is reflected in the Husimi projections of the eigenstates. In the regions where the adiabatic branches are intact one obtains regular Husimi projections concentrated around the phase space orbits of the integrable adiabatic reference Hamiltonians (9). Typical examples of such regular projections corresponding to equal spin projections $c_\uparrow = c_\downarrow$ for the energetic overlap region with two adiabatic branches present are shown in Fig. 3(a) and Fig. 3(b). In Fig. 3(a) the Husimi projection corresponding to an eigenstate in the upper adiabatic potential is shown, whereas in Fig. 3(b) a projection associated with an eigenstates of the lower adiabatic potential is displayed. Sequences of such projections clearly attributable to the coexistence of two independent adiabatic branches were observed until the mixing region is reached. Then Husimi projections incorporating the phase space features of both adiabatic potentials are observed, as shown in Fig. 3(c).

A closer inspection of these projections in the mixing region shows that although the distribution is concentrated on the regular phase space orbits of the adiabatic potentials, the intensity between these parts varies in an irregular and random way, when Husimi projections for a sequence of eigenstates are considered. The structure of the eigenstates which shows up in the random shift of intensity in the Husimi projections is a source of spectral randomness in the absorption bands. In the case of the parameter set A, however, this region of an irregular and random shift of the

phase space distribution is not reached by the absorption processes. In this case the absorption band is located in the region, where the two adiabatic branches are still intact and no spectral mixing between their eigenstates occurs.

In the case of the parameter set B one finds a situation, where the spectral window, which is cut by the transition matrix elements of the absorption process, reaches the region of an irregular mixing of adiabatic states. The Husimi projections for selected eigenstates and equal spin projections which correspond to such a region and which are relevant as final states of an optical transition are shown in the set of Fig. 4(a)-(c). One observes a random variation of the intensity in the Husimi distributions of the eigenstates between the orbits of the two adiabatic potentials. As we show in the next section, as a consequence of this random variation intensities of lines for optical transitions terminating in these states vary randomly.

IV. ABSORPTION

In the calculation of the optical absorption the dimer system is assumed to be small compared to the optical wavelength. Then the electric field vector is approximately equal at the monomer sites of the dimer configuration, i.e. $\vec{E}_n(t) = \vec{E}(t)$. Introducing the projections μ_n of the monomer transition matrix elements onto the direction of the field polarization, i.e. $\vec{E}(t)\vec{\mu}_n = E(t)\mu_n$, ($n = 1, 2$), the interaction of the dimer with the incident light wave is represented in the form

$$\hat{H}_{int} = E(t)\hat{M}_{int}, \quad (18)$$

where \hat{M}_{int} is the interaction operator

$$\hat{M}_{int} = \sum_n |n\rangle\mu_n\langle 0|. \quad (19)$$

In the ground state there is no excitonic-vibronic interaction, i.e. the ground state of the system $|g\rangle$ is given by the direct product of the excitonic vacuum $|0\rangle = |exc0\rangle$ and the vibrational ground state. For the ground state of the vibrational subsystem we assume the zero temperature case, where it is in its lowest state $|m=0\rangle$, with $|m=0\rangle$ the $m=0$ Hermitian polynomial of the undisplaced Q oscillator. Then $|g\rangle = |exc0\rangle|m=0\rangle$. For the optical transition matrix element $M_{\lambda g} = \langle \lambda | \hat{M}_{int} | g \rangle$ of the interaction operator (19), which corresponds to an absorption process from the ground state g into an excited state λ , one then obtains using eq.(13) the expression

$$M_{\lambda g} = \mu_1 c_{\uparrow 0}^{(\lambda)} + \mu_2 c_{\downarrow 0}^{(\lambda)}. \quad (20)$$

The matrix element (20) is representable in the form of a particular projection of the spin vector associated with the $m=0$ vibrational state in (13), $|s_0^{(\lambda)}\rangle$. Introducing the angles

$$\cos \alpha = \frac{\mu_1}{\sqrt{\mu_1^2 + \mu_2^2}}, \sin \alpha = \frac{\mu_2}{\sqrt{\mu_1^2 + \mu_2^2}} \quad (21)$$

and a spin vector $|s_\mu\rangle$ defined by

$$|s_\mu\rangle = \begin{pmatrix} \cos \alpha \\ \sin \alpha \end{pmatrix}, \quad (22)$$

one represents (20) in the form

$$M_{\lambda g} = \sqrt{\mu_1^2 + \mu_2^2} \langle s_\mu | s_0^{(\lambda)} \rangle. \quad (23)$$

Measuring the square of (23), i.e. the absorption strength of an optical transition from $|g\rangle$ to $|\lambda\rangle$, in units of $(\mu_1^2 + \mu_2^2)$ one finds for the dimensionless absorption strength $Q_{\lambda g}$

$$Q_{\lambda g} = \frac{M_{\lambda g}^2}{\mu_1^2 + \mu_2^2} = (\langle s_\mu | s_0^{(\lambda)} \rangle)^2. \quad (24)$$

Comparing eq.(24) with the expression for the Husimi projection (15) it follows that $Q_{\lambda g}$ is equal to a Husimi projection of the λ -eigenstate of (3) taken at the phase space point $Q = P = 0$ with the spin projection being fixed

at s_μ : For $Q = P = 0$ one obtains $\alpha(Q, P) = 0$, which selects the $m = 0$ term in the sum of (15), inserting the value s_μ for the spin vector s , one finds that $h_\lambda(0; s)$ reduces to the r.h.s. of eq.(24), i.e.

$$Q_{\lambda g} = h_\lambda(0; s_\mu). \quad (25)$$

Eq. (25) is in line with the Franck-Condon principle for optical transitions: The transition is vertical from the ground state region at $Q = P = 0$ in the phase space representation and probes the intensity of the final state by its Husimi distribution in the same region. The optical transition matrix elements of the monomers define the spin projection s_μ . For the special case of a symmetric dimer with $\mu_1 = \mu_2$ the transition occurs into the symmetric combination of monomer states. Differences in the optical transition matrix elements, i.e. $\mu_1 \neq \mu_2$, introduce a second asymmetry parameter besides that of the site energy asymmetry ϵ_- . These differences in the optical transition matrix elements express the optical asymmetry of the dimer and enter the optical dimer matrix element (20) through the spin projections (21).

In Fig. 5(a) the absorption bands $Q_{\lambda g}$ calculated from the numerically obtained eigenstates for the parameter set A are represented as stick spectra. Absorption bands are located in accordance with the Franck-Condon principle. This is seen by comparing their positions with the final states following from the adiabatic potentials in (8) by setting $Q = 0$. One finds an energetically lower band for optical transitions terminating in the lower adiabatic potential and a higher band for transitions occurring into the region of the overlap of the two potentials. The shape of the lower band on the left side of Fig. 5(a) is completely regular. The lines of the higher band on the right side of Fig. 5(a) are also regularly arranged. A closer inspection of the higher band, however, reveals that between the lines shown in Fig. 5(a) lines with a much weaker intensity are embedded, which form another regular band. This is evident from the inset, Fig. 5(b), where parts of the lines of the weak and strong bands are shown together. In order to make the weak band visible in the inset a much smaller intensity scale is used. The two bands, into which the absorption spectrum of the high energy part resolves, are easily identified as to belong to the states of the two coexisting adiabatic branches analyzed in the preceding section for the parameter set A: The weak band with relatively small intensities is due to optical transitions terminating in the high energy states of the lower potential (the sign of the Bloch variables of the final states is $x_\lambda > 0$ in accordance with the sign of the lower adiabatic branch (12)), whereas the strong band with much greater intensities is due to optical transitions into the low energy states of the upper potential (for these states $x_\lambda < 0$, again in accordance with the sign of the adiabatic branch (12)).

In Fig. 6 the absorption bands are shown for the parameter set B. The bands are located in the spectral regions of the Franck-Condon energies indicated by the arrows in Fig. 1. The lower absorption band, shown on the left side of the Fig. 6, is regular like the lower band in the Fig. 5(a). The higher band, displayed on the right side of Fig. 6, however, is completely irregular and cannot be resolved into independent subbands as in the case of the parameter set A. This is a consequence of the mixing of the adiabatic reference systems and the irregular structure of the eigenstates analyzed by the Husimi projections in the preceding section. In particular, these projections (see Fig. 4) show a random variation of the intensity in the $Q = P = 0$ region, which according to eq.(25) is relevant for the final states of the optical transitions. This random variation is probed by optical transition matrix elements and results in an irregular pattern of lines in the fine structure of the high energy absorption band.

The absorption bands in Fig. 5 and Fig. 6 were calculated for equal optical transition matrix elements at the monomers $\mu_1 = \mu_2$, which correspond to spin projections of the eigenstates with equal components. The changes occurring in the lower and upper absorption bands in the limiting cases of an optical asymmetry with $\mu_1 \neq 0, \mu_2 = 0$ and $\mu_1 = 0, \mu_2 \neq 0$ for the case of the parameter set B are compared in the Figs. 7 (a) and (b), respectively. These limiting cases correspond to an optical asymmetry, when one of the monomers constituting the dimer is optically active only. Then according to eq.(20) the optical transition matrix element is determined by either the spin up $c_{\uparrow 0}^{(\lambda)}$ or the spin down $c_{\downarrow 0}^{(\lambda)}$ coefficients of the λ eigenstate. As is seen from Fig. 7, which is representative for the case of a positive sign of the excitation energy asymmetry ϵ_- ($\epsilon_- = 10 > 0$ in the case shown in Fig. 7), the lower and upper bands show a redistribution of their intensities with the optical asymmetry: For the given sign of the excitation energy asymmetry $\epsilon_- > 0$ ($\epsilon_- < 0$) the intensity of the upper band is increased (decreased) compared to the symmetric case, $\mu_1 = \mu_2$, displayed in Fig. 6. The lower band behaves in the opposite way, the peak intensities of both bands differing by a factor of about 10^{-3} . In particular, maximum absorption is reached for the high energy band, when the monomer with the higher excitation energy is optically active only, i.e. $\epsilon_- > 0$ with $\mu_1 \neq 0$ and $\mu_2 = 0$. Reversing the optical activity of the monomers but still considering the same asymmetry in the excitation energies, i.e. $\epsilon_- > 0$ with $\mu_1 = 0$ and $\mu_2 \neq 0$, one finds maximum absorption for the low energy band (if $\epsilon_- < 0$, the quantities μ_1 and μ_2 have to be interchanged in the above consideration). As in the case of equal transition matrix elements the lower bands shown on the left sides of Fig. 7(a) and Fig. 7(b) display a regular fine structure, whereas the fine structure of the upper bands, displayed on the right sides of Fig. 7(a) and Fig. 7(b) is irregular. We note that the appearance of the weak bands is due to the coupling of the excited states of both monomers: The monomer, which is optically not active, is still present in the absorption spectrum due to the coupling of the excited states in the dimer system. In the case

displayed on the right side of Fig. 7(b), e.g. an optically nonactive monomer with a high excitation energy attached to an optically active monomer with a lower excitation energy produces a weak but irregular band in the dimer system. A closer inspection of the fine structure of the irregular bands for the limiting cases of an optical asymmetry, in Fig. 7(a) and Fig. 7(b), together with the irregular band for the symmetric case, shown in Fig. 6, reveals that the sequence of lines with a strong and small absorption strength is almost identical in all bands, there is only a small overall change in the line intensities in all three representations. The reason behind this behavior becomes evident after an inspection of the ratio of the spin projections

$$r^{(\lambda)} = c_{\downarrow 0}^{(\lambda)} / c_{\uparrow 0}^{(\lambda)}, \quad (26)$$

which is presented in Fig. 8 as a function of the eigenstate energy E_λ for the spectral regions corresponding to the lower and upper absorption bands, respectively. As is evident from Fig. 8 $r^{(\lambda)}$ is a smooth function of the energy E_λ in the spectral regions of both bands. In particular, for the case of the irregular upper absorption bands, for which in a sequence of eigenstates the spin projection coefficients $c_{\uparrow 0}^{(\lambda)}$ and $c_{\downarrow 0}^{(\lambda)}$ vary in an irregular way, their ratio $r^{(\lambda)}$ considered between neighbouring eigenstates is practically identical. This correlation between the spin up and spin down ($c_{\uparrow 0}^{(\lambda)}$ and $c_{\downarrow 0}^{(\lambda)}$) coefficients results in an almost smooth interpolation of the fine structure of the absorption bands between the limiting cases displayed in the Fig. 7. The smoothness of the function $r^{(\lambda)}$ can be used to express the absorption strength for arbitrary optical asymmetry by one of the limiting cases. For example, representing the down coefficients $c_{\downarrow 0}^{(\lambda)}$ by the up coefficients $c_{\uparrow 0}^{(\lambda)}$ in (20) using eq. (26), one obtains

$$Q_{\lambda g} = \frac{(\mu_1 + \mu_2 r^{(\lambda)})^2}{\mu_1^2 + \mu_2^2} Q_{\lambda g}^+, \quad (27)$$

where $Q_{\lambda g}^+ = [c_{\uparrow 0}^{(\lambda)}]^2$ is the absorption strength for the case $\mu_1 \neq 0$ and $\mu_2 = 0$. The smoothness of the ratio of the different spin projections $r^{(\lambda)}$ together with eq. (27) allows an interpolation between absorption bands for different optical asymmetries. In particular, using this ratio in the prefactor in front of $Q_{\lambda g}^+$ the relative intensities of absorption bands corresponding to different optical asymmetries can be determined.

V. CONCLUSIONS

The transition from the coexistence to a mixing of the adiabatic branches in the eigenstates of a symmetry-broken spin-boson Hamiltonian can be controlled by Bloch and Husimi projections and it shows up in the structure of absorption bands in excitonic-vibronic coupled dimer systems with asymmetric adiabatic potential configurations. In the mixing region of the adiabatic branches phase space distributions of the eigenstates are concentrated on the phase space orbits of both adiabatic potentials and their intensity varies in a random and irregular way. This random variation in the intensity distribution of the eigenstates is probed by the optical transition matrix elements and it is a source of spectral randomness in the fine structure of the absorption bands. The asymmetry of the optical transition matrix elements of the dimer configuration is representable by suitably chosen spin projections of the spin part of the eigenstates. In the limiting cases of the optical asymmetry, in which one of the monomers constituting the dimer is optically active only, the intensities of the absorption lines are determined by either the spin up or spin down coefficients. For the states relevant for the optical absorption correlated spin down and spin up coefficients are obtained. As a result the shape of the fine structure of the irregular absorption bands remains almost the same for different optical asymmetries. Finally we point out that in the case of a symmetry-broken spin-boson Hamiltonian optical absorption processes can probe the high energy regions of the overlap of adiabatic potentials where it is possible to observe a transition from regular to irregular absorption spectra for asymmetric molecular dimer configurations.

- [1] L. Müller, J. Stolze, H. Leschke, and P. Nagel, Phys. Rev. A 55, 1022 (1991).
- [2] H. Schanz, and B. Esser, Phys. Rev. A 44, 3375 (1997).
- [3] G. Stock, and M. Thoss, Phys. Rev. Lett. 78, 578 (1997).
- [4] R. Steib, J. L. Schoendorff, H. J. Korsch, and P. Reineker, Phys. Rev. E 57, 6534 (1998).
- [5] J. S. Briggs, and A. Herzenberg, Molecular Physics 23, 203 (1972).

- [6] M. Sonnek, H. Eiermann, and M. Wagner, Phys. Rev. B 51, 905 (1995).
- [7] U. Rempel, B. von Maltzan, and C. von Borczyskowski, J. Lumin. 53, 175 (1992).
- [8] K. Takahashi, Progr. Theor. Phys. Suppl. 98, 109 (1989).
- [9] W. A. Lin, and L. E. Ballentine, Phys. Rev. Lett. 65, 2927 (1990)
- [10] M. B. Cibils, Y. Cuche, P. Leboef, and W. F. Wreszinski, Phys. Rev. A 46, 4560 (1992).
- [11] M. Kus, Phys. Rev. Lett. 54, 1343 (1985).
- [12] M. Cibils, Y. Cuche, and G. Müller, Z. Phys. B 97, 565 (1995).
- [13] H. Schanz, and B. Esser, Z. Phys. B 101, 299 (1996).
- [14] Th. Zimmermann, H. Köppel, L. S. Cederbaum, G. Persch, and W. Demtröder, Phys. Rev. Lett. 61, 3 (1988)

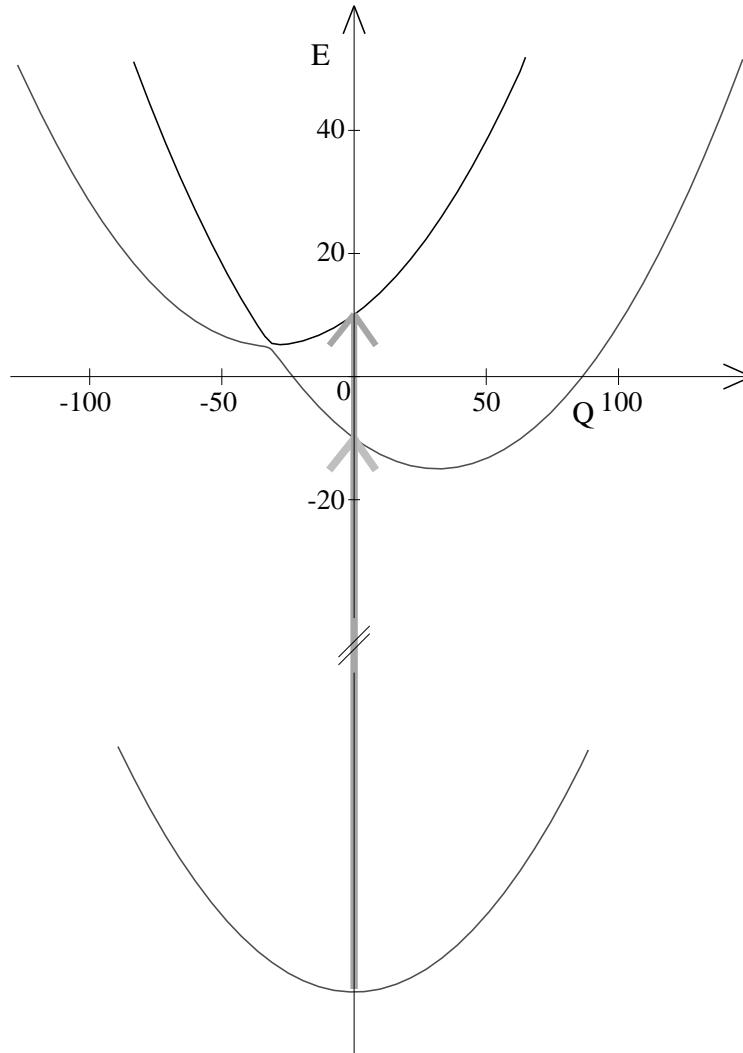


FIG. 1. Asymmetric adiabatic potentials and ground state configuration for the parameter set B. In the case of the parameter set A the asymmetry in the configuration of the adiabatic potentials is similar, but less pronounced as compared to B. Arrows mark the location of the absorption bands at the Franck-Condon energies.

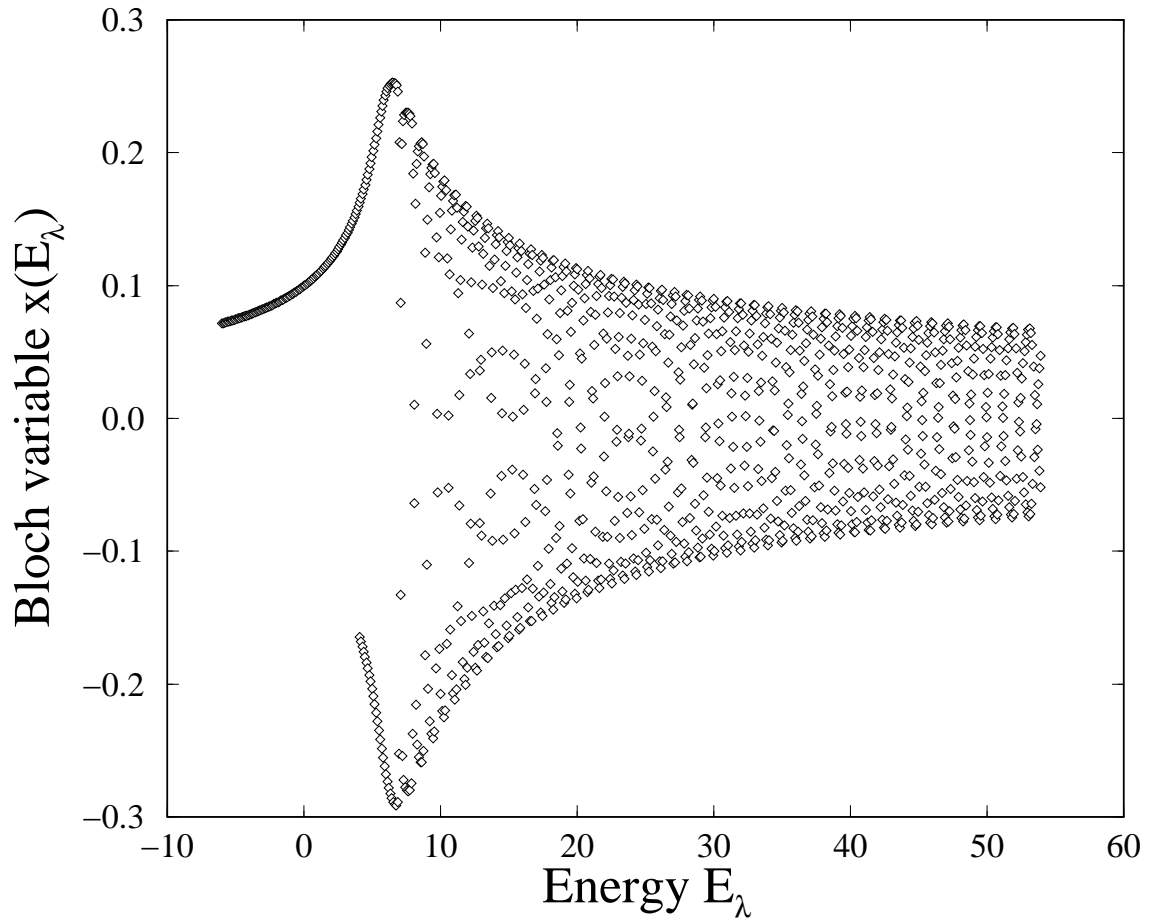


FIG. 2. Bloch projections $x(E_\lambda)$ of the eigenstates for the parameter set A. The presence of three characteristic regions with one adiabatic branch, coexistence of two adiabatic branches and the mixing region is clearly visible. The Bloch projections for the parameter set B show a similar behavior.

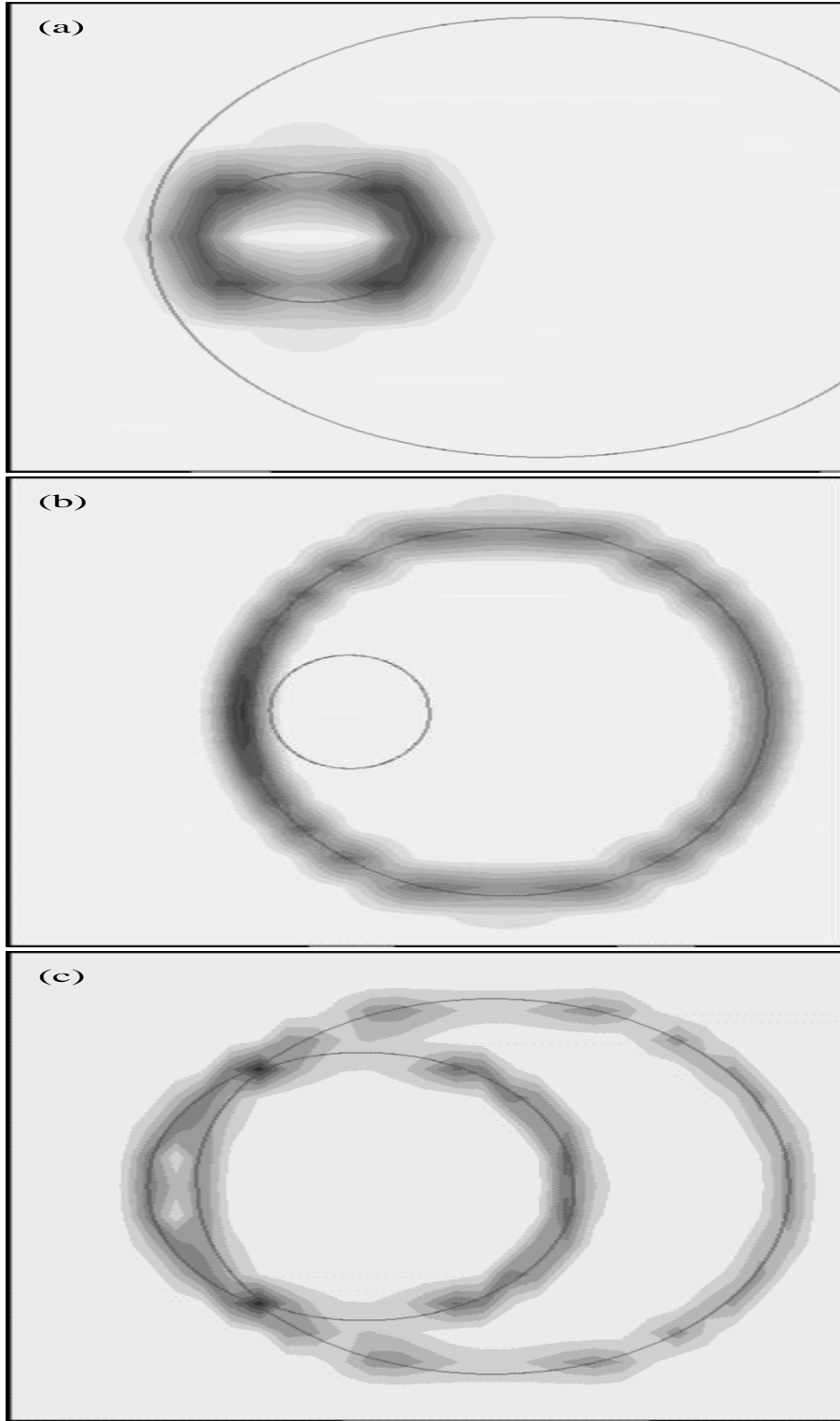


FIG. 3. Husimi projections for the parameter set A in the overlap region of the adiabatic potentials. The solid lines indicate the classical phase space orbits of the adiabatic Hamiltonians (9). The projections correspond to the eigenstates 120 (a), 121 (b) and 310 (c), with the eigenstate energies $E_{120} = 5.0028$, $E_{121} = 5.0956$ and $E_{310} = 14.5176$, respectively. The selected phase space parts are (a): $-50 \leq Q \leq 50$, $-5 \leq P \leq 5$, (b): $-75 \leq Q \leq 75$, $-6 \leq P \leq 6$ and (c): $-90 \leq Q \leq 90$, $-8 \leq P \leq 8$, with the Q-axis displayed horizontally and P-axis displayed vertically. The projections in (a) and (b) are located on the phase space orbits of the upper and lower adiabatic potentials, respectively, and show the coexistence of both adiabatic branches in the selected energy interval. The projection (c) is located on the phase space orbits of both adiabatic potentials and characteristic for the mixing region of the adiabatic reference states in the spectrum.

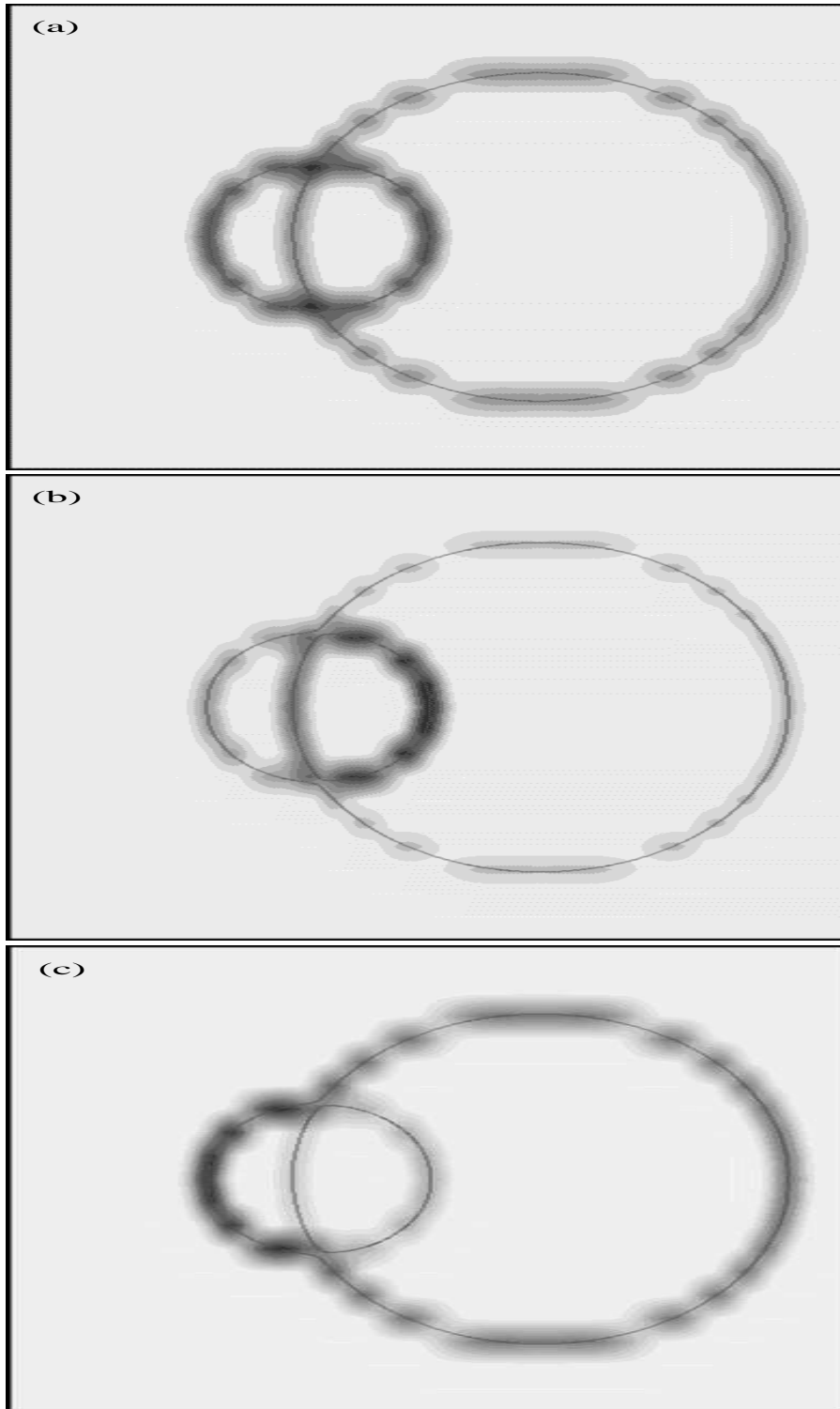


FIG. 4. Husimi projections for the parameter set B. The solid lines indicate the classical phase space orbits of the adiabatic Hamiltonians (9). The projections correspond to the eigenstates 300 (a), 302 (b) and 303 (c), with the eigenstate energies $E_{300} = 10.0237$, $E_{302} = 10.1467$ and $E_{303} = 10.1520$, respectively. In all projections the selected phase space parts are $-120 \leq Q \leq 120$, $-10 \leq P \leq 10$, with the Q-axis displayed horizontally and P-axis displayed vertically. The projections are located on the phase space orbits of both adiabatic potentials and characteristic for the mixing of adiabatic reference states. One observes a random variation in the intensity of the distribution between the different eigenstates. This random variation includes the center of the rectangle, i.e. the region around $Q = P = 0$, which is the final state region for the upper absorption band shown in Fig.6. The different intensities in this region correspond to different strengths of the absorption lines of the upper band in Fig.6.

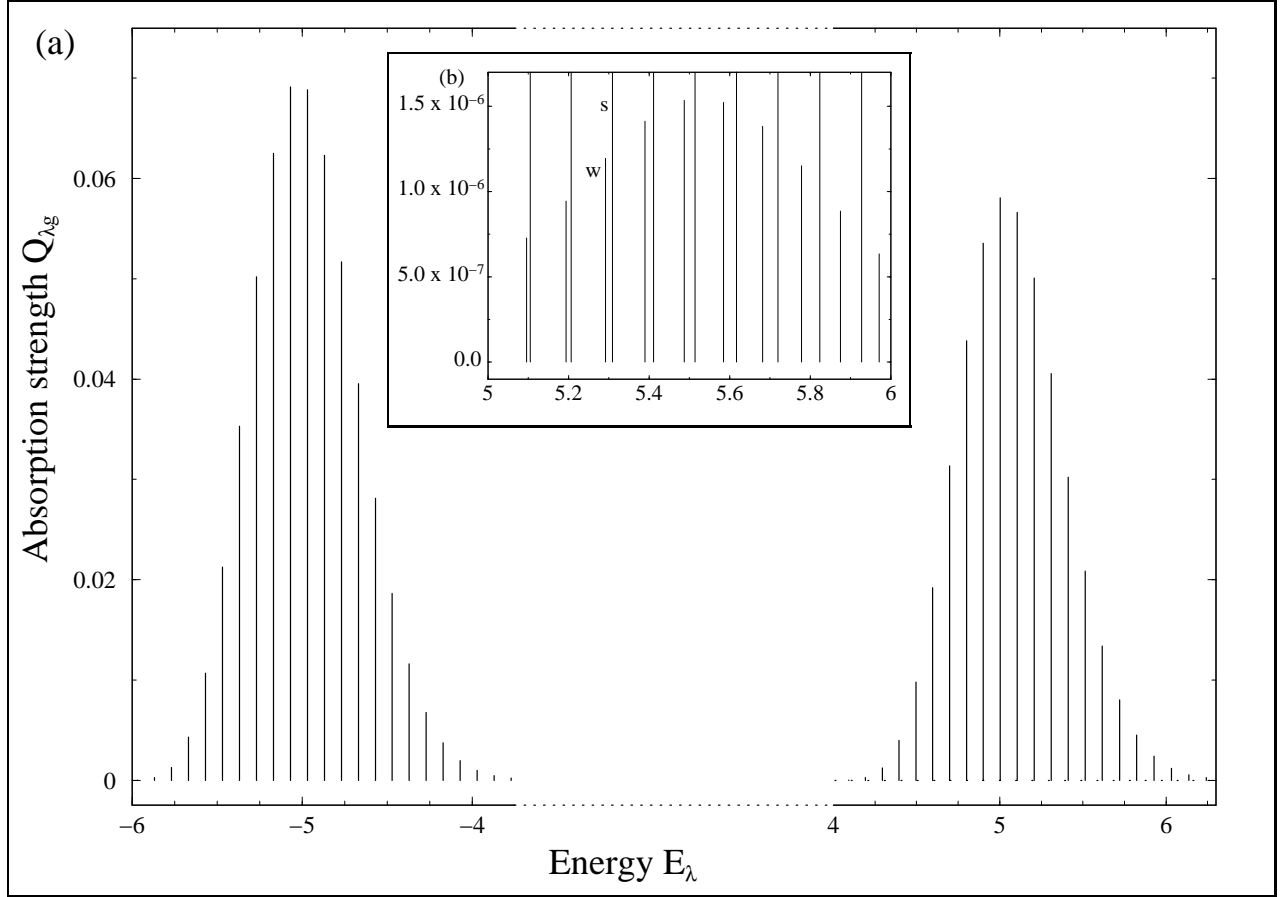


FIG. 5. Lower and upper absorption bands for the parameter set A. In (a) the strong intensity lines of the upper band are visible only. A closer inspection of the upper band shows that this band is a superposition of two regular bands corresponding to the final states in the upper and lower potential and the coexistence of two independent adiabatic branches in this part of the spectrum. This superposition becomes evident from the inset (b), in which a change of scale is used to display the weak lines, which are embedded between the strong lines (not drawn to peak intensity and cut off at the upper edge). In the inset a pair of neighbouring weak and strong lines are indicated by the labels w and s, respectively.

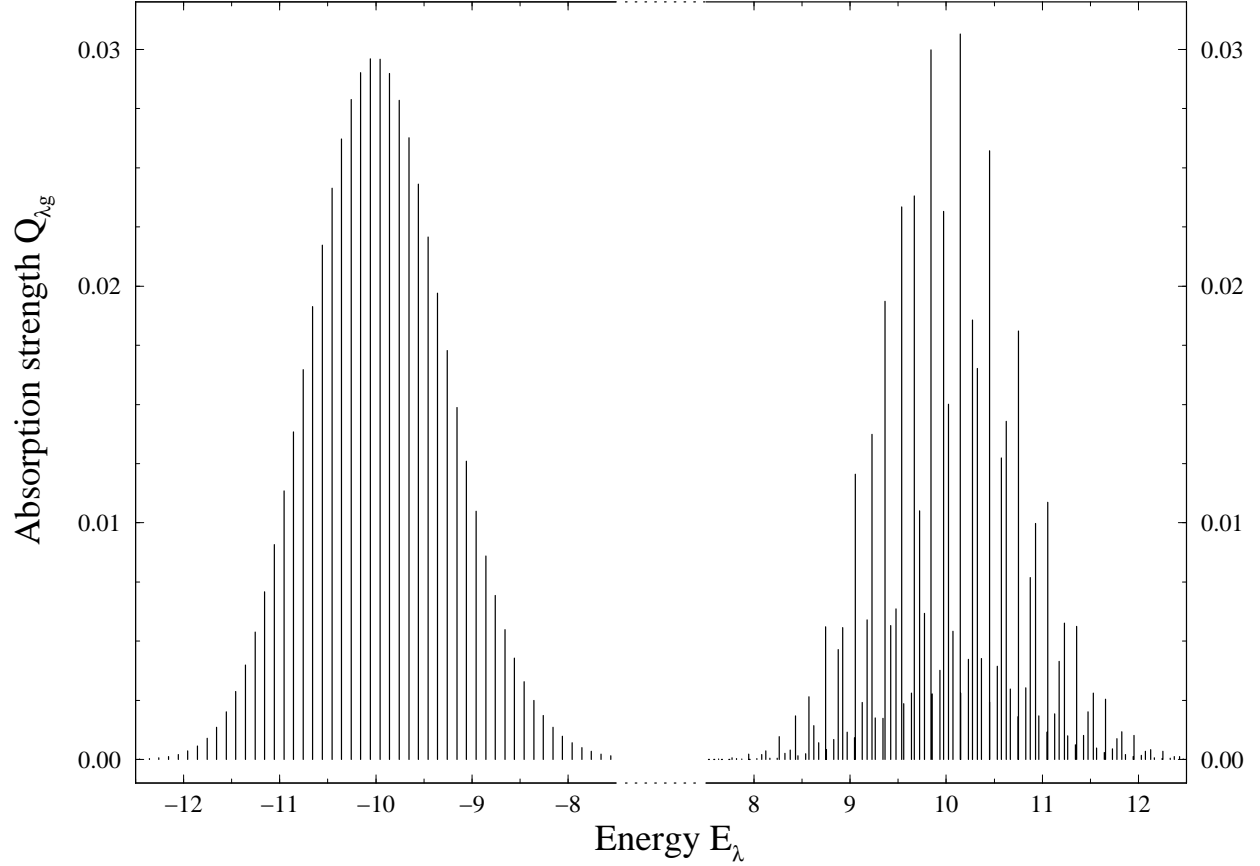


FIG. 6. Lower and upper absorption bands for the parameter set B and the case of optical symmetry, $\mu_1 = \mu_2$. A broken energy scale is used to display both bands. The lower band is regular with final states in the lower adiabatic potential, whereas the upper band is irregular due to the mixing of the adiabatic reference states, compare with the intensity variation in the Husimi projections displayed in Fig. 4.

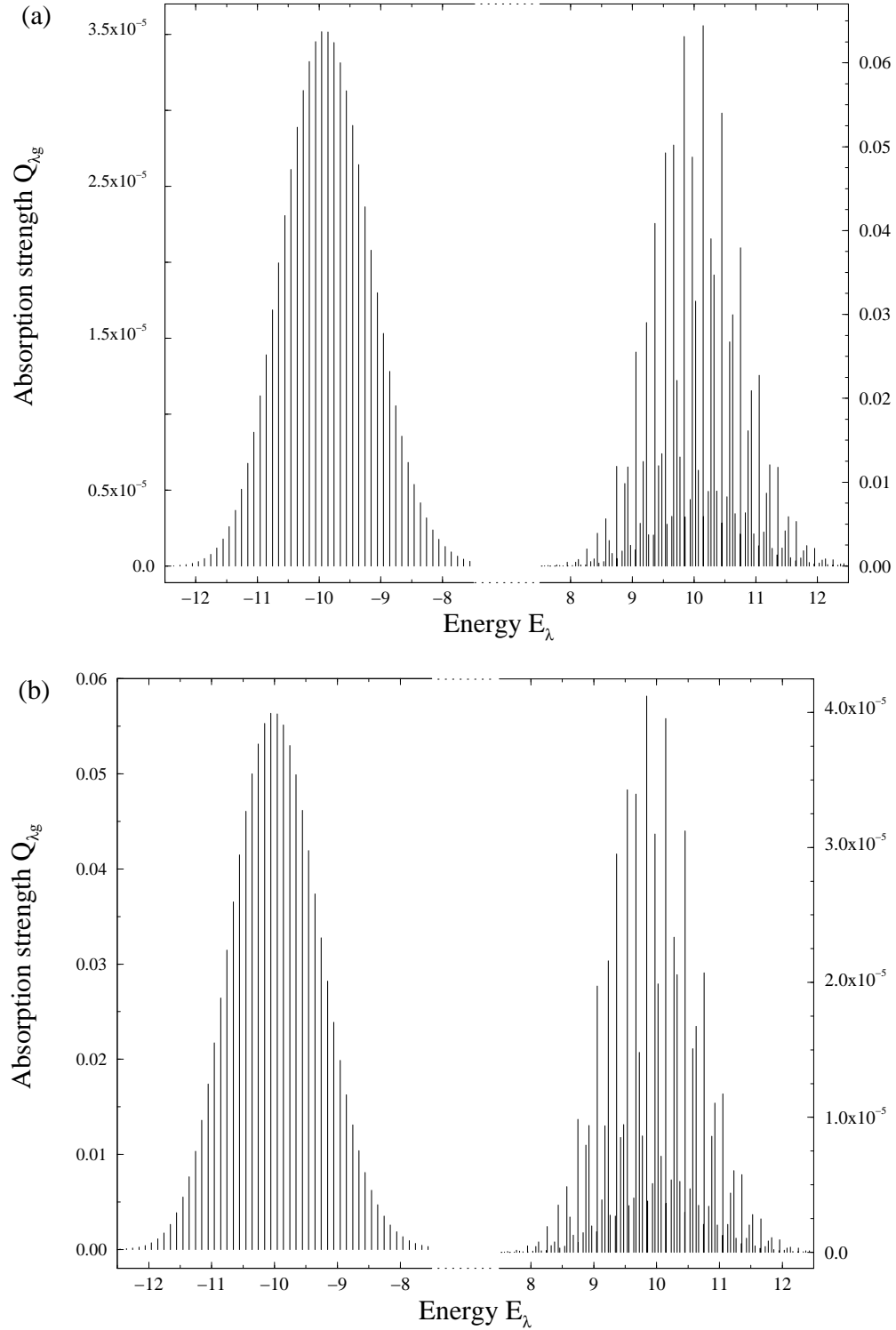


FIG. 7. Absorption bands for the parameter set B in the limiting cases of optical asymmetry, when one of the molecules of the dimer is optically active only: $\mu_1 \neq 0, \mu_2 = 0$ (shown in part (a)) and $\mu_2 \neq 0, \mu_1 = 0$ (shown in part (b)). Note the differences between the overall intensities of the lower and upper bands as indicated by the scales on the left and right hand sides, respectively: In (a) the intensity of the lower band is by three orders of magnitude smaller than the upper band, in (b) the intensities of the bands are reversed. Independent of this change in intensity the upper bands in both (a) and (b) are irregular and have a similar fine structure.

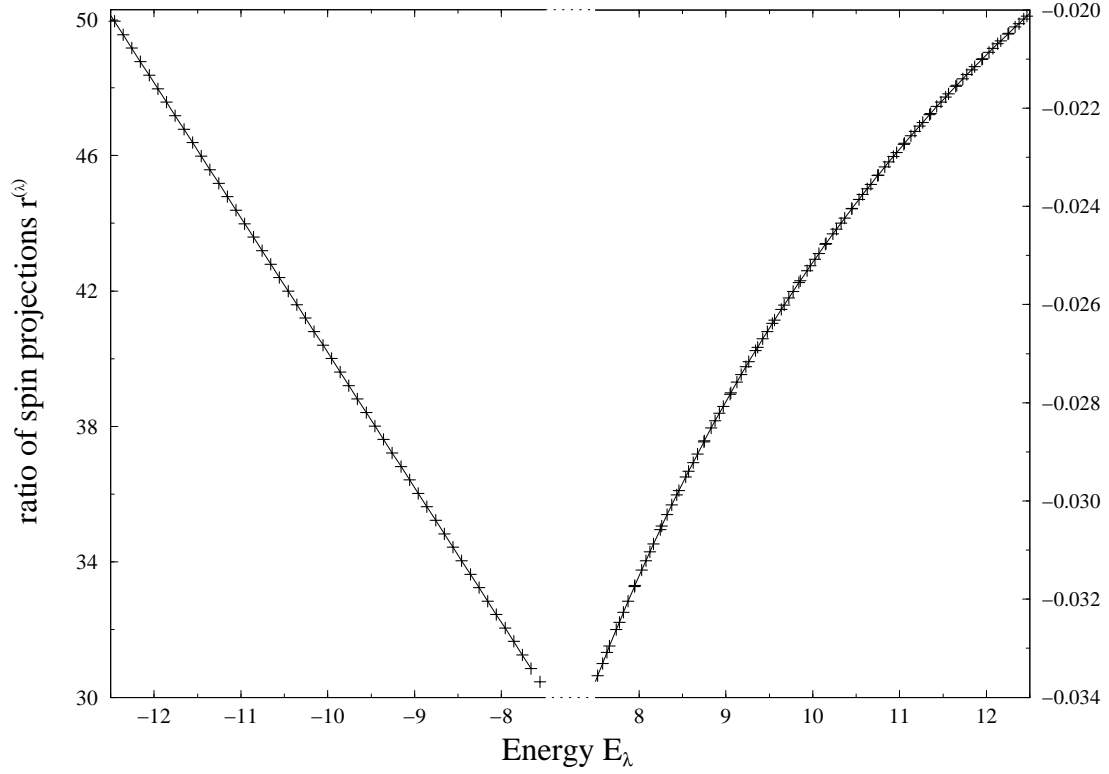


FIG. 8. Ratio of the spin down to spin up coefficients $r^{(\lambda)}$ in the spectral regions of the lower and upper absorption bands of Fig. 7. The scales on the left and right side correspond to the ratios in the region of the lower and upper band, respectively. Note the smooth dependence of $r^{(\lambda)}$ on the eigenstate energy in the spectral region of the upper absorption bands, despite the irregular structure of the upper bands in Fig. 6 and Fig. 7 (a),(b).